PHOTONICS Research

X-ray absorption spectroscopy study of energy transport in foil targets heated by petawatt laser pulses

I. Y. Skobelev,[1,2] S. N. Ryazantsev,[1,3] D. D. Arich,[1,2] P. S. Bratchenko,[1,2] A. Y. Faenov,[1,4] T. A. Pikuz,[1,5] P. Durey,[6] L. Doehl,[6] D. Farley,[6] C. D. Baird,[6] K. L. Lancaster,[6] C. D. Murphy,[6] N. Booth,[7] C. Spindloe,[7] P. McKenna,[8] S. B. Hansen,[9] J. Colgan,[10] R. Kodama,[4,5] N. Woolsey,[6] and S. A. Pikuz[1,2,*]

[1]Joint Institute for High Temperatures, RAS, Moscow 125412, Russia
[2]National Research Nuclear University "MEPhI," Moscow 115409, Russia
[3]M. V. Lomonosov Moscow State University, Moscow 119991, Russia
[4]Open and Transdisciplinary Research Initiative, Osaka University, Osaka 565-0871, Japan
[5]Graduated School of Engineering, Osaka University, Osaka 565-0871, Japan
[6]York Plasma Institute, Department of Physics, University of York, York YO10 5DD, UK
[7]Central Laser Facility, STFC Rutherford Appleton Laboratory, Didcot OX11 0QX, UK
[8]Department of Physics, SUPA, University of Strathclyde, Glasgow G4 0NG, UK
[9]Sandia National Laboratories, Albuquerque, New Mexico 87123, USA
[10]Theoretical Division, Los Alamos National Laboratory, Los Alamos, New Mexico 87545, USA
*Corresponding author: spikuz@gmail.com

Received 13 November 2017; revised 26 December 2017; accepted 27 December 2017; posted 3 January 2018 (Doc. ID 313362); published 2 March 2018

X-ray absorption spectroscopy is proposed as a method for studying the heating of solid-density matter excited by secondary X-ray radiation from a relativistic laser-produced plasma. The method was developed and applied to experiments involving thin silicon foils irradiated by 0.5–1.5 ps duration ultrahigh contrast laser pulses at intensities between 0.5×10^{20} and 2.5×10^{20} W/cm^2. The electron temperature of the material at the rear side of the target is estimated to be in the range of 140–300 eV. The diagnostic approach enables the study of warm dense matter states with low self-emissivity.

OCIS codes: (280.5395) Plasma diagnostics; (300.1030) Absorption; (300.6560) Spectroscopy, x-ray.
https://doi.org/10.1364/PRJ.6.000234

1. INTRODUCTION

The investigation of high-temperature plasmas at near-solid densities produced by powerful short laser pulses is pursued to increase the fundamental understanding of atomic and equations-of-state properties of material at high-energy density [1,2] and for developing several important applications, such as fast ignition of thermonuclear fusion targets [3–5] and the creation of bright radiographic sources [6,7]. Petawatt (PW) lasers with relativistic flux values efficiently generate electron beams with energies up to hundreds of megaelectronvolts (MeV) in solid-density targets. In turn, those fast electrons penetrate the target to a depth of tens of micrometers, resulting in rapid heating of the material. The temperatures the inner layers of the target material reach depend on the target material, the laser intensity, and the layer depth. In Refs. [8,9], for example, temperatures on the order of 220–450 eV were measured at submicrometer depths, while in Ref. [10] values of $T_e \sim$ 500 eV were obtained at depths of ~15 μm.

There is no comprehensive theory of solid target heating. Until recently, it was believed that the main mechanism for energy transfer from the relativistic electron beam to the solid target was ohmic heating by return currents [11]. More recent work reported by Sherlock *et al.* [12] suggests that the collisional damping of high-amplitude plasma waves excited by the relativistic electron beam can become the dominant heating mechanism. Any comprehensive model needs to take into account, for example, the resistive properties of the material [13], magnetic field generated by plasma currents, small-scale filamentation of electrons due to the Weibel instability [14], and the presence of a laser prepulse. Extracting experimental measurements from

high-energy-density matter, particularly when the temperatures are low, i.e., in warm dense matter, is difficult, as the material is typically opaque (even for X-ray radiation) and too cool to emit in the X-ray regime. The most successful methods use layered foil targets to combine materials of different atomic numbers at the front and the rear sides and then analyze the self-emission from the target rear [10]. Yet these targets are complex due to resistivity changes at the interface between material layers. Here we demonstrate X-ray absorption spectroscopy as a powerful tool for exploring the warm dense matter state. The method deals with homogeneous single-material targets in the form of planar foils. As X-ray emission from the hot, laser-irradiated material at the front of the target passes through the remainder of target, it reveals the parameters of much less-heated regions whose own emissivity is too low to be registered. While temperature gradients in the sample may be expected to complicate any quantitative analysis, we find that a simple two-region model captures the essential features of the measured data.

2. CALCULATIONS OF THE ABSORPTION AND EMISSION PROPERTIES OF PLASMA

The analysis methodology divides the target foil into two layers—A and B—as shown in Fig. 1. Layer A is directly exposed to the laser radiation and acquires a high bulk electron temperature in the range of 500–1000 eV for laser intensity on the order of 10^{20} W/cm^2. Absorbing plasma Layer B with a thickness d_B is located next to Layer A, but deeper in the target; this layer has a lower electron temperature $T_{e,B}$. Two focusing spectrometers with spatial resolution (FSSR) [15,16] are arranged to detect the radiation emanating from the front and the rear surfaces of the foil, as shown in Fig. 1. The first spectrometer, indicated on the right-hand side in Fig. 1, records the spectrum $S_f(\lambda)$ emitted by Layer A from the front (laser-irradiated surface) of the target, and the second spectrometer (left-hand side in Fig. 1) records emission from the rear surface.

The rear-surface emission is the sum of the emission from Layers A, which is partially absorbed in Layer B, and from Layer B itself,

$$S_r(\lambda) = S_B(\lambda) + P_B(\lambda) S_f(\lambda), \quad (1)$$

where $P_B(\lambda)$ is the spectral transmittance of Layer B. In Eq. (1), the emission contribution from Layer B to the front-side spectra is neglected since the temperature of Layer B, and consequently its emittance in X-rays, will be negligible compared

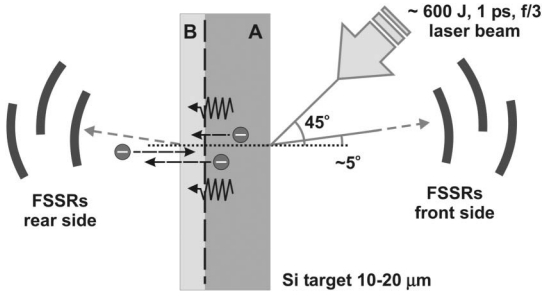

Fig. 1. Experimental layout showing the division of single material target split into Layers A and B and the location of the front and rear spectrometers.

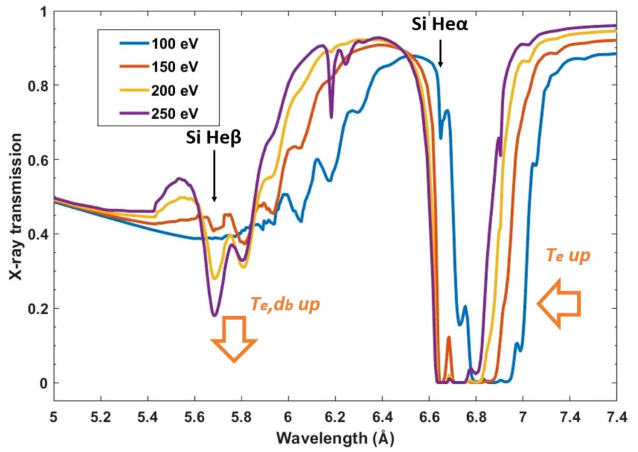

Fig. 2. Spectral transmission $P_B(\lambda)$ calculated for different temperatures and constant plasma layer thickness of $d_B = 10$ μm.

to the emission from Layer A. In Eq. (1), the values $S_r(\lambda)$ and $S_f(\lambda)$ are directly measured, while $S_B(\lambda)$ and $P_B(\lambda)$ are calculated using steady-state collisional-radiative kinetic atomic physics. Only two input parameters, $T_{e,B}$ and d_B, are needed for this calculation. As this approach uses an intense, short laser pulse, the heating of Layer B is nearly isochoric (i.e., constant volume) over the short timescale of its interaction with hot electrons. Consequently, Layer B remains near solid density, with an electron density determined by the temperature and the average ion charge, which is calculated using a collisional-radiative model. Thus, diagnosing the parameters of Layer B reduces to finding $T_{e,B}$ and d_B by reaching the best fit to the measured $S_r(\lambda)$ from the collisional-radiative calculations and Eq. (1).

To produce synthetic spectra representing absorption in Layer B, we use the PrismSPECT atomic kinetics and spectral synthesis software [17]. The present model calculates collisional ionization, recombination, excitation and deexcitation, photo-recombination, radiative decay, dielectronic recombination, and autoionization rates among 11,481 states of silicon including all possible charge states. These rates are used to find steady-state level populations and produce synthetic absorption spectra. Radiation transfer was taken into account in the approximation of the Biberman–Holstein escape factors for a planar plasma. The spectral transmission coefficient takes into account all possible processes of photon absorption due to free-free, bound-free, and bound-bound transitions. Figure 2 shows examples of calculated spectral transmittance coefficients $P_B(\lambda)$ for various temperatures. It can be seen that the form of $P_B(\lambda)$ proves to be very sensitive to the value of $T_{e,B}$, which makes the proposed diagnostic technique possible. The most remarkable feature is a shift of the absorption edge in the wavelength range of 6.8–7.0 Å while changing the temperature from 100 to 250 eV in the absorption layer.

3. EXPERIMENTAL SETUP

The experiments were made at the Vulcan Petawatt facility at the Rutherford Appleton Laboratory. Vulcan PW facility generates a laser beam using optical parametric chirped-pulse amplification (OPCPA) technology at a central wavelength

of 1054 nm to deliver to the target a pulse duration of full width at half-maximum (FWHM) of ~0.7 ps. The OPCPA technology enables an amplified spontaneous emission (ASE)-to-peak-intensity-contrast ratio below 10^{-9}, and an additional plasma mirror was applied to improving the contrast ratio beyond 10^{-10} to ensure the main pulse interacting with an undisturbed cold target and achieve reproducible results.

The typical laser pulse energy measured before the compressor was 600 ± 50 J, while the efficiency of the beam delivery line, including laser compressor, $f/3$ off-axis parabolic mirror, and plasma mirror was measured as 50%, resulting in approximately 300 J laser energy on target. After the p-polarized beam was reflected by plasma mirror, it formed a 7-μm-diameter focal spot at 45° incidence to the target surface normal. The central focal spot contains 30% of the laser energy, resulting in an estimate of 2.3×10^{20} W/cm^2 peak laser intensity.

The X-ray emission from the target was recorded by means of in the directions close to the target surface normal as shown in Fig. 1. In order to obtain spectra with high resolution ($\lambda/\Delta\lambda \approx 4000$) and in a broad range from 4.75 to 7.4 Å, three FSSRs equipped with spherically bent quartz crystals were aligned to adjoined wavelength bands. Spectrometers were precalibrated along the wavelength scale using reference spectral lines obtained from Si ions in low-laser-intensity low-plasma-density laser shots, so the wavelength of the absorbing spectra features was measured with 3 mÅ precision. Additionally, using the intensities of reference lines, the spectrometers were cross-calibrated, so the intensities of their data are directly comparable.

The spectra were recorded by means of Fujifilm TR Image Plate detectors and an Andor DX434 charge-coupled device (CCD) camera. These were protected from exposure to visible light by two layers of 1-μm-thick polypropylene $(C_3H_6)_n$ with a 0.2-μm Al coating, or by a single 25-μm-thick beryllium window. Additionally, to prevent saturation of the detectors, Mylar ($C_{10}H_8O_4$) filters of 1–20 μm thickness were used. This was chosen depending on the requested laser energy and target thickness associated with a particular laser shot. Background fogging and crystal fluorescence due to intense fast electrons were limited using a pair of 0.5-T neodymium-iron-boron permanent magnets that formed a 10-mm-wide slit in front of each crystal.

4. DIAGNOSTIC RESULTS

Each experimental spectrum was analyzed using the method described above, and the extracted values of $T_{e,\mathrm{B}}$ and d_B were found to satisfy Eq. (1) with sufficient accuracy. The modeling precision is demonstrated in Fig. 3, where the measured spectra are compared with the value of $S_{r,\mathrm{mod}}(\lambda) = S_\mathrm{B}(\lambda) + P_\mathrm{B}(\lambda)S_f(\lambda)$ for experiments with foils of different thicknesses and at different laser pulse energies. It should be noted that despite the simplicity of the model used, the procedure describes experimental spectra with robust accuracy. This implies that the temperature gradient in the cool layer responsible for X-ray absorption is not large, and the absorption properties of Layer B can be described by a single temperature. We note that the results are consistent with the conclusion in Ref. [10], where matter was heated above 500 eV at a depth of 15 μm inside a solid by a laser pulse of similar intensity and pulse duration.

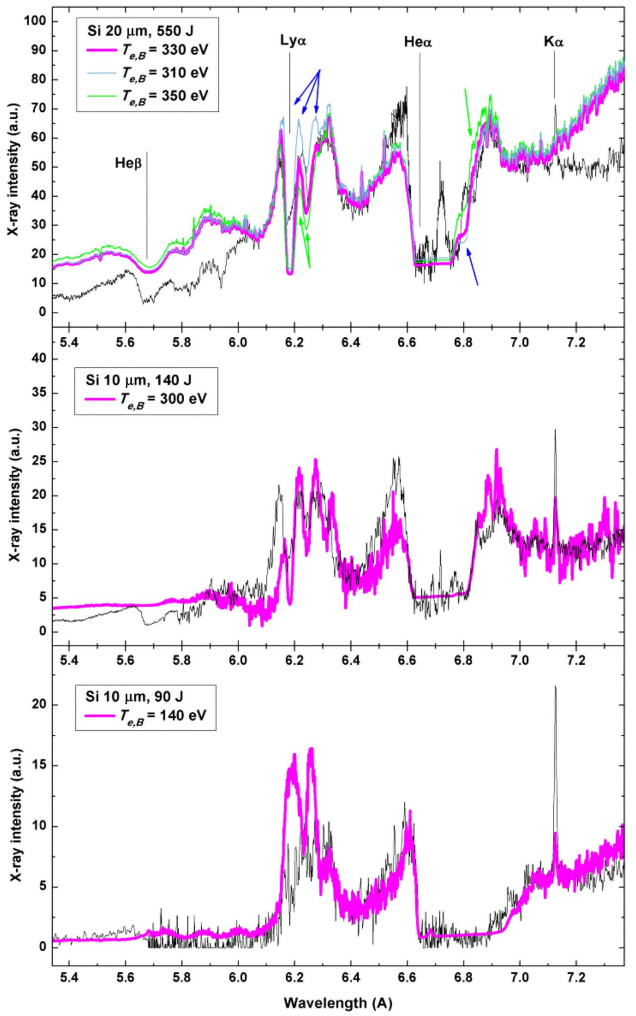

Fig. 3. X-ray spectra measured from the rear sides of Si foil targets with different thicknesses (black thin lines) and best fit modeled (thick purple lines) for temperatures $T_{e,\mathrm{B}}$ from 140 to 330 eV and absorbing plasma layer thickness $d_\mathrm{B} = 5$ μm. Spectral calculations at temperatures that differ from the best-fit value are shown by the thin blue lines and indicate the uncertainty in the current method.

As seen in Fig. 3, the temperature of Layer B at the rear of the target ranges from 140 to 330 eV with the average temperature decreasing with decreasing laser intensity. The targets had different thicknesses, and the value of the absorbing plasma layer d_B was adjusted to account for the observed amplitude of the absorption lines. The result was $d_\mathrm{B} = 5$ μm in each case. Aside of the best-fit cases, in upper panel of Fig. 3 two modeled spectra calculated for plasma layer temperatures that deviated between 310 eV and 350 eV are given. As these spectra provide clearly less correspondence to the experimental data in the range of 6.1–6.4 Å (H-like ion absorption), the given deviated temperatures can be considered as an upper estimate for error bars of the method.

Note that at temperatures below ~100 eV the self-emission from a silicon plasma is so weak that K-shell emission spectroscopy is impossible.

Despite the good qualitative agreement between the modeled and observed spectra, there are several deficiencies.

The observed neutral K_α line (wavelength ~7.125 Å) is not reproduced by the model. This line is probably emitted by fast electrons reaching a cold area of the target located at a distance from the center of the laser focal spot. At lower laser energy of 90–100 J, the modeled spectra and experimental ones do not match at around ~6.2 Å wavelength. This is linked to the absorption on the 1s–2p transition in the H-like Si XIV ion, which is not seen in the modeled spectra and most likely arises due to temporal gradients. In particular, the largest amount and the highest emittance of H-like Si ions occurs at the time of maximum temperature in Layer A. This is also the time of the highest temperature in the cooler and absorbing Layer B. This is when the populations of emitting (Layer A) and absorbing (Layer B) H-like ions are most transient. It is important to note that a simple single-layer absorber model successfully captures many features of a spectrum over a range of conditions in otherwise difficult-to-diagnose warm dense materials. This model provides information on the spatial scale and temperature dependence of the warm dense matter created.

5. CONCLUSIONS

In this paper, we proposed a method for extracting the temperature of warm dense matter in near-solid conditions using an X-ray absorption spectroscopy technique with no target modifications. The method was developed and applied in experiments with flat silicon foils irradiated by 0.7–1.5-ps ultrahigh-contrast laser pulses of $0.5–2.5 \times 10^{20}$ W/cm^2 intensities. The electron temperature of the warm dense matter created at the rear side of the target was estimated to be in the range of 140–330 eV. It should be noted that the measured temperatures are in good accordance with the results of 2D particle-in-cell simulations described in Ref. [18]. The advantages of the diagnostic approach include the possibility to diagnose warm dense matter with a low self-emissivity for both homogeneous and layered targets.

Funding. Russian Science Foundation (RSF) (17-72-20272); Science and Technology Facilities Council (STFC) (EP/L000644/1); Engineering and Physical Sciences Research Council (EPSRC) (EP/L01663X/1); Los Alamos National Laboratory (LANL); National Nuclear Security Administration (NNSA); U.S. Department of Energy (DOE) (DE-AC5206NA25396).

Acknowledgment. The work of JIHT RAS team on X-ray data measurements and analysis is funded by RSF. The work of UK team is funded by STFC and EPSRC. The LANL is operated by Los Alamos National Security, LLC for the NNSA of the U.S. DOE.

REFERENCES

1. D. J. Hoarty, P. Allan, S. F. James, C. R. D. Brown, L. M. R. Hobbs, M. P. Hill, J. W. O. Harris, J. Morton, M. G. Brookes, R. Shepherd, J. Dunn, H. Chen, E. Von Marley, P. Beiersdorfer, H. K. Chung, R. W. Lee, G. Brown, and J. Emig, "Observations of the effect of ionization-potential depression in hot dense plasma," Phys. Rev. Lett. **110**, 265003 (2013).
2. S. J. Rose, "The radiative opacity at the Sun centre—a code comparison study," J. Quantum Spectrosc. Radiat. Transfer **71**, 635–638 (2001).
3. S. Y. Gus'kov, N. N. Demchenko, N. V. Zmitrenko, P. A. Kuchugov, V. B. Rozanov, R. V. Stepanov, and R. A. Yakhin, "Fast ignition of asymmetrically compressed targets for inertial confinement fusion," J. Exp. Theor. Phys. Lett. **105**, 402–407 (2017).
4. M. Tabak, J. Hammer, M. E. Glinsky, W. L. Kruer, S. C. Wilks, J. Woodworth, E. M. Campbell, M. D. Perry, and R. J. Mason, "Ignition and high gain with ultrapowerful lasers*," Phys. Plasmas **1**, 1626–1634 (1994).
5. R. Kodama, P. A. Norreys, K. Mima, A. E. Dangor, R. G. Evans, H. Fujita, Y. Kitagawa, K. Krushelnick, T. Miyakoshi, N. Miyanaga, T. Norimatsu, S. J. Rose, T. Shozaki, K. Shigemori, A. Sunahara, M. Tampo, K. A. Tanaka, Y. Toyama, T. Yamanaka, and M. Zepf, "Fast heating of ultrahigh-density plasma as a step towards laser fusion ignition," Nature **412**, 798–802 (2001).
6. T. A. Pikuz, A. Y. Faenov, S. V. Gasilov, I. Y. Skobelev, Y. Fukuda, M. Kando, H. Kotaki, T. Homma, K. Kawase, Y. Hayashi, T. Kawachi, H. Daido, Y. Kato, and S. V. Bulanov, "Propagation-based phase-contrast enhancement of nanostructure images using a debris-free femtosecond-laser-driven cluster-based plasma soft X-ray source and an LiF crystal detector," Appl. Opt. **48**, 6271–6276 (2009).
7. M. Nishiuchi, H. Sakaki, T. Z. Esirkepov, K. Nishio, T. A. Pikuz, A. Y. Faenov, I. Y. Skobelev, R. Orlandi, A. S. Pirozhkov, A. Sagisaka, K. Ogura, M. Kanasaki, H. Kiriyama, Y. Fukuda, H. Koura, M. Kando, T. Yamauchi, Y. Watanabe, S. V. Bulanov, K. Kondo, K. Imai, and S. Nagamiya, "Towards a novel laser-driven method of exotic nuclei extraction-acceleration for fundamental physics and technology," Plasma Phys. Rep. **42**, 327–337 (2016).
8. A. Saemann, K. Eidmann, I. E. Golovkin, R. C. Mancini, E. Andersson, E. Förster, and K. Witte, "Isochoric heating of solid aluminum by ultrashort laser pulses focused on a tamped target," Phys. Rev. Lett. **82**, 4843–4846 (1999).
9. K. Eidmann, U. Andiel, F. Pisani, P. Hakel, R. C. Mancini, G. C. Junkel-Vives, J. Abdallah, and K. Witte, "K-shell spectra from hot dense aluminum layers buried in carbon and heated by ultrashort laser pulses," J. Quant. Spectrosc. Radiat. Transfer **81**, 133–146 (2003).
10. R. G. Evans, E. L. Clark, R. T. Eagleton, A. M. Dunne, R. D. Edwards, W. J. Garbett, T. J. Goldsack, S. James, C. C. Smith, B. R. Thomas, R. Clarke, D. J. Neely, and S. J. Rose, "Rapid heating of solid density material by a petawatt laser," Appl. Phys. Lett. **86**, 191505 (2005).
11. A. R. Bell, J. R. Davies, S. Guerin, and H. Ruhl, "Fast-electron transport in high-intensity short-pulse laser—solid experiments," Plasma Phys. Controlled Fusion **39**, 653–659 (1997).
12. M. Sherlock, E. G. Hill, R. G. Evans, S. J. Rose, and W. Rozmus, "In-depth plasma-wave heating of dense plasma irradiated by short laser pulses," Phys. Rev. Lett. **113**, 255001 (2014).
13. V. T. Tikhonchuk, "Interaction of a beam of fast electrons with solids," Phys. Plasmas **9**, 1416–1421 (2002).
14. M. Honda, J. Meyer-ter-Vehn, and A. Pukhov, "Two-dimensional particle-in-cell simulation for magnetized transport of ultra-high relativistic currents in plasma," Phys. Plasmas **7**, 1302–1308 (2000).
15. Y. S. Lavrinenko, I. V. Morozov, S. A. Pikuz, and I. Y. Skobelev, "Reflectivity and imaging capabilities of spherically bent crystals studied by ray-tracing simulations," J. Phys. **653**, 012027 (2015).
16. M. A. Alkhimova, S. A. Pikuz, A. Y. Faenov, and I. Y. Skobelev, "Determination of spectral reflectivity of spherically bent mica crystals applied for diagnostics of relativistic laser plasmas," J. Phys. **774**, 012115 (2016).
17. J. J. Macfarlane, I. E. Golovkin, P. R. Woodruff, D. R. Welch, B. V. Oliver, T. A. Melhorn, and R. B. Campbell, "Simulation of the ionization dynamics of aluminum irradiated by intense short-pulse lasers," in *Inertial Fusion Sciences and Applications 2003 (IFSA 2003): State of the Art*, B. A. Hammel, D. D. Meyerhofer, J. Meyer-ter-Vehn, and H. Azechi, eds. (American Nuclear Society, 2004), p. 457.
18. D. Wu, X. T. He, W. Yu, and S. Fritzsche, "Particle-in-cell simulations of laser-plasma interactions at solid densities and relativistic intensities: the role of atomic processes," arXiv: 1703.05127 (2017).